S 1 → S n and S 2 → S n Absorption of Azulene: Femtosecond Transient Spectra and Excited State Calculations

ARTICLE *in* THE JOURNAL OF PHYSICAL CHEMISTRY A · MARCH 2003

Impact Factor: 2.69 · DOI: 10.1021/jp021313e

4 AUTHORS, INCLUDING:

Paolo Foggi
Università degli Studi di Perugia
119 PUBLICATIONS **1,641** CITATIONS
SEE PROFILE

Frederik Neuwahl
European Commission
19 PUBLICATIONS **967** CITATIONS
SEE PROFILE

$S_1 \rightarrow S_n$ and $S_2 \rightarrow S_n$ Absorption of Azulene: Femtosecond Transient Spectra and Excited State Calculations

Paolo Foggi[†]

Dipartimento di Chimica, Università di Perugia, Via Elce di Sotto 8, 06123 Perugia, Italy

Frederik V. R. Neuwahl

Laboratorio Europeo di Spettroscopie non Lineari (LENS), Dipartimento di Fisica, Università di Firenze, via N. Carrara 1, 50019 Sesto Fiorentino, Firenze, Italy

Laura Moroni and Pier Remigio Salvi*

Dipartimento di Chimica, Università di Firenze, via della Lastruccia 3, 50019 Sesto Fiorentino, Firenze, Italy

Received: May 30, 2002; In Final Form: December 2, 2002

The transient spectra of azulene in solution have been measured in the spectral region 600−350 nm at room temperature, pumping into the S_1 and S_2 states with femtosecond pulses and probing with a delayed femtosecond white light continumm. The spectra are a combination of ground-state bleaching, stimulated emission, and excited-state absorption. The latter component gives a direct information on excited states which may be not active in the ground-state absorption. $S_1 \rightarrow S_n$ and $S_2 \rightarrow S_n$ absorptions have been discussed with the help of ab initio calculations of the MCSCF/CAS type with the 6-31G* basis set and including perturbative corrections. The calculated $S_0 \rightarrow S_n$, $S_{1,eq} \rightarrow S_n$, and $S_{2,eq} \rightarrow S_n$ vertical excitation energies and oscillator strengths are in satisfactory agreement with the experimental results. It has been found that electronic states, weakly active in the ground-state absorption, occur with high intensity in the femtosecond transient spectra, in particular in the energy range 36000−44000 cm^{-1} above the ground-state energy.

I. Introduction

Azulene, the nonalternant aromatic isomer of naphthalene, is known to have unusual photophysical properties.[1−8] In contrast with the vast majority of aromatic molecules which show $S_1 \rightarrow S_0$ fluorescence under low excitation intensity,[9] azulene fluoresces from the second excited state to S_0 with quantum yield $\eta_{S_2 \rightarrow S_0} = 0.046$ in cyclohexane solution at room temperature[10] and to S_1 ($\eta_{S_2 \rightarrow S_1} \approx 4 \times 10^{-6}$) in methylcyclohexane glass at 77 K[8,11] while only very weakly from S_1 to S_0 ($\eta_{S_1 \rightarrow S_0} < 10^{-6}$) with laser excitation.[7] The depopulation process from S_1 in condensed media has been extensively investigated with subpicosecond pump−probe experiments.[12−20] In the most recent study,[20] the S_1 decay time of azulene in cyclohexane solution was accurately determined as a function of the excess vibrational energy above the S_1 origin, decreasing from 1.7 ps at the origin to ≈0.4 ps 1300 cm^{-1} higher. The radiationless decay was related to the occurrence of a S_1/S_0 conical intersection.[21] Experimental evidence for the energetic location of the conical intersection has been recently obtained for azulene in condensed phase[20] and in jet-cooled conditions.[22] On the other hand, the fluorescent S_2 state is relatively long-lived, ≈1−1.6 ns in common solvents.[10]

Time-resolved absorption with spectrally broad probe pulses having femtosecond/picosecond time duration (white light continuum)[23−26] may in principle give information both on the relaxation dynamics and on the spectroscopy of excited states. In the past few years, the technique has been in fact widely applied to a variety of fast dynamical processes, including internal conversion,[27−31] intramolecular excited-state proton[32,33] and electron[34] transfer, and valence tautomeric interconversion.[35] Transient absorption of azulene is here measured to access electronic states not active in the ground state absorption, once the contribution of excited state absorption (ESA) to the overall signal is extracted. Sampling regions of energy surfaces different from those responsible for the ground state absorption enables us to acquire independent sets of spectral data which may be usefully compared with theoretical predictions. In fact, ab initio calculations of ESA have been already proposed in order to predict materials which have optimal characteristics with respect to important technical applications such as optical limiting.[36]

II. Experimental Section

Azulene from Aldrich (99% nominal purity) was used without further purification. Standard absorption and fluorescence (λ_{exc} = 313 nm) spectra of azulene 4×10^{-5} M in cyclohexane are in complete agreement with reference data.[9,37] Azulene solutions in cyclohexane were freshly prepared at the concentration 10^{-1} M and 5×10^{-3} M to pump into S_1 and S_2 states, respectively. Under our excitation conditions, the fraction of molecules promoted to the excited states is estimated to be ≈1−3%.

The experimental instrumentation and data processing for time-resolved studies in the femtosecond time regime have been described in detail in previous papers.[26,30] In short, the ultrashort pulses (≤70 fs at 800 nm) from a Ti:sapphire laser are stretched, amplified at 1 kHz repetition rate by means of a regenerative

* To whom correspondence should be addressed. E-mail: piero.salvi@unifi.it.

[†] Also at Laboratorio Europeo di Spettroscopie non Lineari (LENS), Dipartimento di Fisica, Università di Firenze, via N. Carrara 1, and at INFM, Unitá di Firenze, via G. Sansone 1, 50019 Sesto Fiorentino, Firenze, Italy.

10.1021/jp021313e CCC: $25.00
Published on Web 00/00/0000 PAGE EST: 7.1

amplifier, and then recompressed (90−100 fs; ≈700 mW). The amplified pulse train is divided into two portions, the most intense of which generates, through parametric generation and amplification into a BBO crystal,[38] signal and idler output. In the present experiment, the second harmonic of the signal at the wavelength of maximum conversion efficiency, 680 nm, pumps azulene directly into the S_1 state. To pump directly into the S_2 state, the fourth harmonic of the signal is generated, providing 3−6 μJ at 340 nm. The weakest portion, 2−5 μJ at 800 nm, is directed onto a CaF_2 plate and produces a slightly chirped white light continuum of femtosecond pulses from 350 up to ≈750 nm, which is further split into two parts of equal intensity by a 50/50 fused silica Al beam splitter. One of these, acting as probe beam, measures the transient transmittance at any given delay time with respect to the excitation beam. The second, travelling along a shorter optical path, interacts with the same volume of the sample seen by the excitation and probe beams before the excitation process and therefore provides a convenient reference signal. The remaining intensity of the 800 nm light, still much larger than that of the white continuum, is carefully filtered out of the whole beam before probe and reference reach the sample. Because of the absence of filters in early transient absorption experiments pumping into S_2 azulene,[39] the pump beam mixed nonlinearly with the 800 nm beam producing an efficient dumping of the population from S_2 to S_1. The observed transient spectrum, incorrectly assigned to the $S_2 \rightarrow S_n$ transition,[39] is actually due to S_1. On the other hand, to avoid saturation effects on the detector because of the high pump intensity, a short-wave pass filter is inserted along the beam path after incidence on the sample, thus reducing the upper limit of the transient spectrum to ≈650 nm.

The signal detection is operated by means of a back-illuminated CCD camera with spectral response in the range 300−1000 nm. Two horizontal strips covering ∼300 nm are selected on the CCD target to collect the probe and reference signals spectrally dispersed after passing through a flat field 25 cm Czerny-Turner spectrograph.

The transient transmittance at a given delay time τ and wavelength λ, $T(\tau,\lambda)$, is defined as $I(\tau,\lambda)/I_0(\lambda)$, where $I(\tau,\lambda)$ and $I_0(\lambda)$ are the intensities of the white light continuum reaching the detector with and without the pump pulse.[26,27] To take advantage of the reference intensity, $I_r(\lambda)$, two measurements are performed, the first with the probe beam only, thus acquiring $I_r(\lambda)$ and $I_0(\lambda)$ and then the baseline signal, and the second with both the excitation and probe beams, enabling us to know $I(\tau,\lambda)$ and $I_r(\lambda)$. In this case, the transient transmittance $T(\tau,\lambda)$ is obtained as $[I(\tau,\lambda)/I_r(\lambda)]\times[I_r(\lambda)/I_0(\lambda)]$. In kinetic studies, for small variations of $T(\tau,\lambda)$ it is usual to express the transient optical density $\Delta OD \simeq [1 - T(\tau,\lambda)]/2.303$. To prevent any effect due to group velocity mismatch (GVM) between pump and probe pulses, the azulene solution flows into a 0.3 mm thin cell in all our experiments. Further, due to chirping of the white light continuum transient spectra were corrected according to the procedure described in ref 26.

III. Excited State Absorption of Azulene

For the sake of clarity, let us first review the most important results on the $S_0 \rightarrow S_n$ spectrum of azulene[40−52] which are pertinent to our study, making reference to Figure 1 for the axis reference system and to Figure 2 for the ground-state absorption spectrum. There are four distinct absorption regions in the azulene spectrum: ≈700−500 nm, 350−310 nm, 290−260 nm, 240−220 nm, with oscillator strengths 0.009, 0.06, ≈1, and 0.4, respectively.[48] The two lowest systems have their electronic origins at 14320 and 28330 cm^{-1} and show well resolved vibronic structures at room temperature. The third, i.e., the strongest band system of azulene, consists of three relatively broad bands at 35 650, 36 350, and 36 770 cm^{-1}. The fourth is a single diffuse absorption centered around 42 100 cm^{-1}. The allowed component of the first and fourth band system are known[2,48] to be short axis (*y*, see Figure 1) polarized, whereas those of the second and third are long-axis (*z*) polarized.[2,47] Interposed between the second and the third band system there is a separate *y*-polarized weak transition[48] at ≈33 800 cm^{-1}. Above 43 000 cm^{-1} (≈220 nm), three others bands are observed in solution, at 48 200, 52500, and 62 600 cm^{-1}, with no definite assignment.[51] These are not however Rydberg excitations, easily observed in this energy range in gaseous azulene but efficiently quenched when azulene is in a condensed phase.[52]

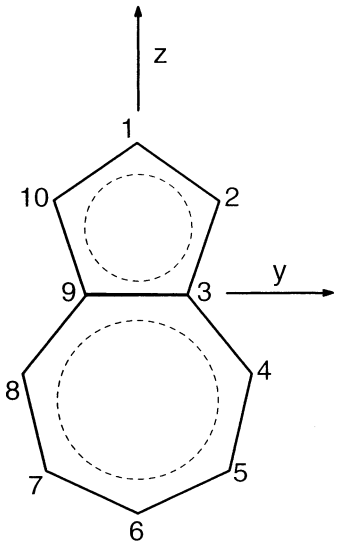

Figure 1. Atom numbering and axis reference system of azulene.

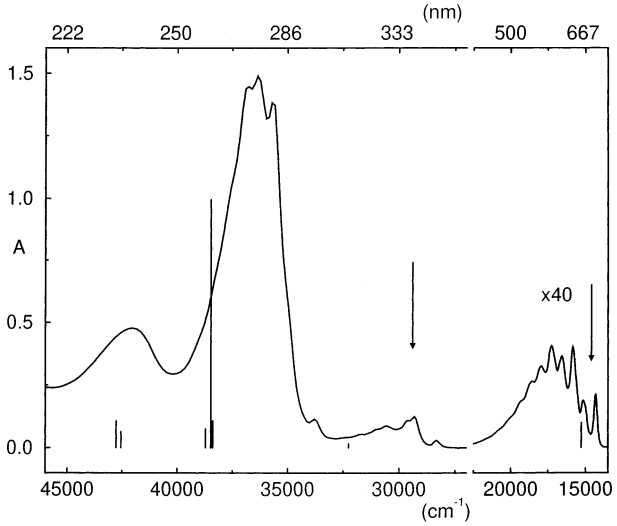

Figure 2. $S_0 \rightarrow S_n$ absorption spectrum of azulene 4×10^{-5} M in cyclohexane solution. Bottom: calculated vertical excitation energies and oscillator strengths of the $S_0 \rightarrow S_n$ transitions, according to our MCSCF/CAS(10,10)/6-31G*/QDPT calculations (see text for details). The pump energies for transient $S_1 \rightarrow S_n$ and $S_2 \rightarrow S_n$ experiments are also indicated in the Figure by vertical arrows.

A. $S_1 \rightarrow S_n$ Spectrum. The transient spectrum of azulene 10^{-1} M in cyclohexane solution, pumping at 680 nm, i.e., ≈400 cm^{-1} above the S_1 origin, and probing with a femtosecond white light continuum pulse, has been measured as a function of the delay time of the probe with respect to the pump pulse. The

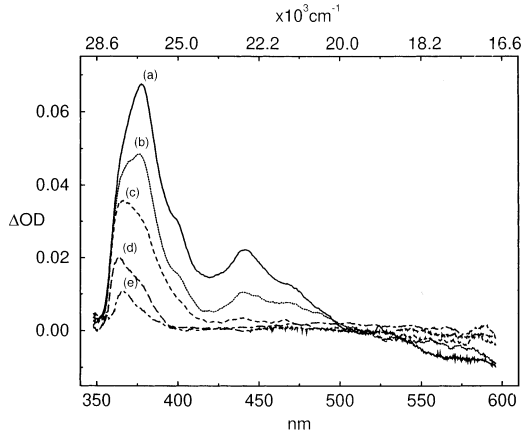

Figure 3. Transient optical density (ΔOD, 350−600 nm spectral range) of azulene 10^{-1} M in cyclohexane at room-temperature pumping at 680 nm after 0.2, 0.65, 1.3, 2.5, and 4 ps delay times [traces a−e, respectively] of the probe with respect to the pump pulse.

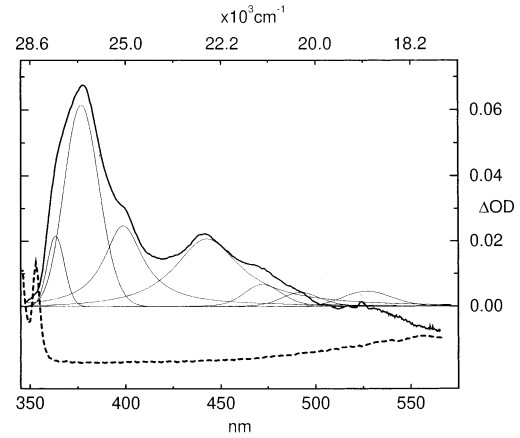

Figure 4. Upper: transient optical density, ΔOD, of azulene (10^{-1} M in cyclohexane, 350−600 nm spectral range, room temperature, 0.2 ps delay time, pump wavelength 680 nm) fitted with seven bands of Gaussian character (see text for details). Lower: the $S_0 \rightarrow S_n$ spectrum (dashed) in the same wavelength range.

time evolution of the transient optical density, ΔOD, in the spectral region 350−600 nm is reported in Figure 3. Negative signals correspond to ground-state bleaching (B) or stimulated emission (SE) processes, whereas positive signals correspond to excited-state absorption (ESA).[34] As the 350−600 nm wavelength range partially overlaps the azulene $S_0 \rightarrow S_1$ (≈500−700 nm) and $S_0 \rightarrow S_2$ (≤360 nm) absorption bands, bleaching in these regions is expected. The effect is easily recognized above ≈500 nm in the transient spectra observed at early delay times by comparison with the ground state absorption, as shown in Figure 4. The bleaching contribution may be estimated more quantitatively considering the spectrum taken at 0.2 ps delay time and assuming that the negative signal at 580 nm is due solely to bleaching. The ESA signal, 680 nm pump plus 580 nm probe energy, i.e., in the region of the S_2 vibronic manifold more than 3000 cm^{-1} above (0−0) S_2-S_0, is expected to be quite small. Within this approximation it may be seen from Figure 4 that the onset of the $S_0 \rightarrow S_2$ absorption band distorts negligibly the transient spectrum. The bleaching component has been subtracted to the experimental spectrum and the resulting profile has been fit to seven Gaussian bands, as shown in Figure 4. The fitting parameters are reported in Table 1.

As to the positive signal, two different absorption mechanisms must be considered. In fact, our results on the relaxation

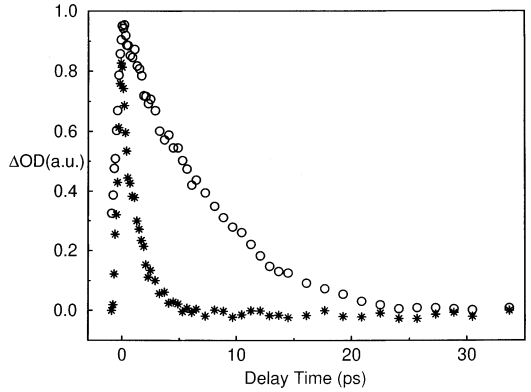

Figure 5. Transient optical density, ΔOD, of azulene 10^{-1} M in cyclohexane at room temperature and with 680 nm pump wavelength as a function of the delay time: asterisks, $\lambda_{probe} = 390$ nm; circles, $\lambda_{probe} = 360$ nm. The two decay curves are normalized to unity.

TABLE 1: Band Centers (ν_0, × 10^3 cm^{-1}), Widths [Γ (fwhm), cm^{-1}], and Oscillator Strengths *f* of the Seven Component Bands, A, B, C, D, E, F, and G, of the Observed Transient Spectrum $S_1 \rightarrow S_n$ Shown in Figure 4

	A	B	C	D	E	F	G
ν_0	19.0	20.3	21.2	22.6	25.1	26.5	27.5
Γ	1170	1140	1220	2140	1560	1800	960
f	1×10^{-5}	6×10^{-6}	1.7×10^{-5}	1.3×10^{-4}	1×10^{-4}	2×10^{-4}	3×10^{-5}

dynamics of azulene transient bands, summarized in Figure 5, indicate the occurrence of two decay mechanisms, both having instantaneous rise time within the time resolution of our experimental apparatus (≈150 fs). The first has time constant ≤1.4 ps probing at 390 and 440 nm, in fair agreement with the most recent measurements.[20] The process has been interpreted as internal $S_1 \rightarrow S_0$ conversion.[12−20] In addition, with probe wavelength around 360 nm, a second decay kinetics is found having a time constant of 8 ps (see Figure 5). Decay times between tens and hundreds of picoseconds have been observed in azulene when exciting in the S_1 manifold and monitoring on the long wavelength edge of higher absorption bands.[54,55] These have been ascribed to ground state deactivation of vibrationally hot molecules once the internal $S_1 \rightarrow S_0$ is completed. This process should be excluded in our case on the basis of the fact that (i) the small excess energy of the pump with respect to the S_1 origin plausibly causes a negligible increase of the internal molecular temperature and (ii) the two observed maxima of Figure 5 are coincident, indicating that the slow decay does not temporally follow internal conversion. The process may be justified noting that the 680 nm pulse not only induces the $S_0 \rightarrow S_1$ transition but also may mix nonlinearly with white continuum pulses, when temporally coincident, to stimulate Raman modes. The CCC bending mode 825 cm^{-1}, strongly active in the resonance Raman spectrum,[53] is a suitable candidate, being available pulses at 720 nm in the white continuum. Probing the vibrational relaxation through hot band $S_0 \rightarrow S_2$ absorption, a transient positive signal is expected to the red of the S_0-S_2 origin around 364 nm, in reasonable agreement with the transient peak observed at delay times as late as 4 ps (see Figure 3).

The ESA spectrum of azulene in cyclohexane at 0.2 ps delay time, resulting from further subtracting the hot band absorption contribution to the transient spectrum, is compared with the $S_0 \rightarrow S_n$ spectrum in Figure 6, setting the ESA starting level at the S_1 origin, 14 320 cm^{-1} above the ground state. Two absorption maxima fall at 269 and 244 nm. The former lies in the region of the third band system and may therefore be confidently assigned as a transition from S_1 to the same final

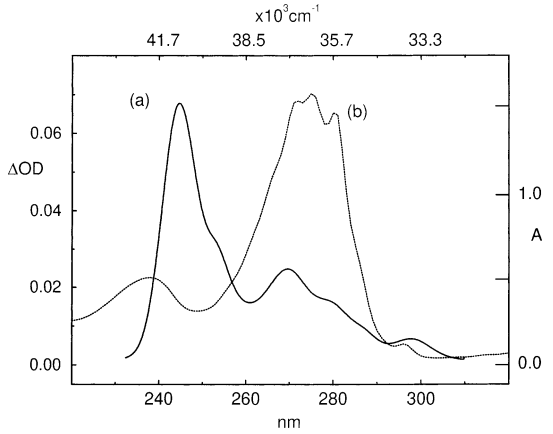

Figure 6. $S_0 \rightarrow S_n$ [(b), *A* units on the right] and ESA $S_1 \rightarrow S_n$ [(a), ΔOD units on the left] spectra of azulene in cyclohexane at room temperature. The ESA spectrum has been obtained from the transient spectrum of Figure 4 (see text for details) and is shifted by 14 320 cm^{-1}, the energy of the (0−0) $S_0 \rightarrow S_1$ transition.

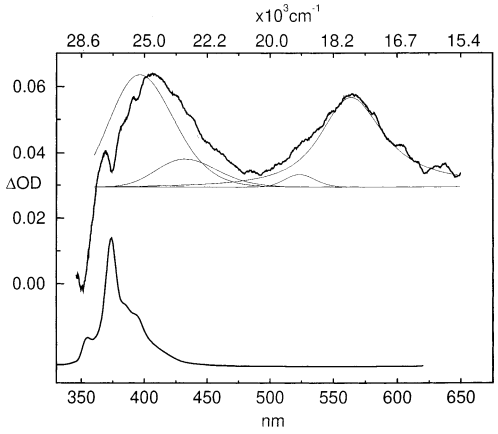

Figure 7. Upper: transient optical density, ΔOD, of azulene (5×10^{-3} M in cyclohexane, 350−650 nm spectral range, room temperature, 15 ps delay time, pump wavelength 340 nm). The contribution of the $S_2 \rightarrow S_0$ stimulated emission has been subtracted from the transient spectrum and the component due to excited-state absorption (ESA) fitted with four bands of Gaussian character (see text for details). Lower: the $S_2 \rightarrow S_0$ fluorescence spectrum.

state. The latter has no clear $S_0 \rightarrow S_n$ counterpart. The ESA/$S_0 \rightarrow S_n$ comparison of Figure 6 suggests also the correspondence of the weak 298 nm band (≈33 500 cm^{-1}) with that at 296 nm (≈33 800 cm^{-1}) in the $S_0 \rightarrow S_n$ spectrum.

Finally, going back to Figure 4 and considering our experimental conditions (active volume ≈10^{-5} cm^{-3}; pulse energy ≈5 μJ at 680 nm; ground-state absorbance of the 0.1 M solution ≈1 at 680 nm), the $S_1 \rightarrow S_n$ extinction coefficient $\epsilon_{S_1 \rightarrow S_n}$ was estimated at 377 nm, i.e., the maximum of the strongest ESA band, to be 400 $l\ mol^{-1}\ cm^{-1}$. Therefrom, the oscillator strengths of the seven bands have been also calculated and reported in Table 1.

B. $S_2 \rightarrow S_n$ Spectrum. Pumping azulene 5×10^{-3} M in cyclohexane solution with 340 nm radiation (≈29 400 cm^{-1}, 1070 cm^{-1} above the S_2 origin) and probing with the white light continuum in the 350−650 nm spectral region, the $S_2 \rightarrow S_n$ transient spectrum is measured (see Figure 7). Ground-state bleaching above ≈500 nm has in this case a negligible effect on the transient spectrum because of the concentration reduction. On the contrary, stimulated $S_2 \rightarrow S_0$ emission may be sizable and, in fact, decreases the positive ESA signal below 400 nm, as it is seen by comparison with the fluorescence $S_2 \rightarrow S_0$ spectrum of azulene, shown in the same figure. Also the band structure visible on the high energy transient band is entirely due to SE. Once this component is subtracted, the ESA spectrum has been fitted to the sum of four Gaussians, shown in the same Figure. The fitting parameters and the oscillator strengths are reported in Table 2, having estimated that the extinction coefficient, $\epsilon_{S_2 \rightarrow S_n}$ at 558 nm is ≈2600 $l\ cm^{-1}\ mol^{-1}$.

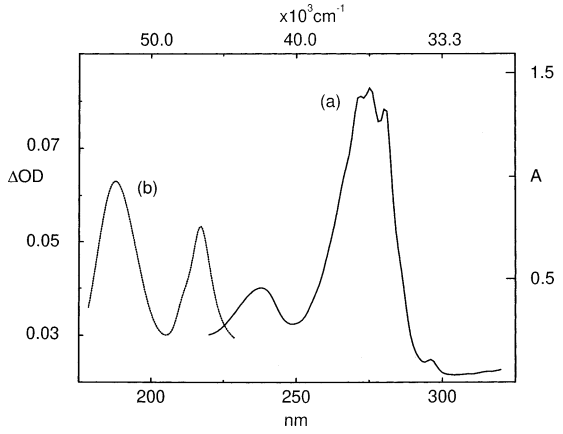

Figure 8. $S_0 \rightarrow S_n$ [(a), *A* units on the right] and ESA $S_2 \rightarrow S_n$ [(b), ΔOD units on the left] spectra of azulene in cyclohexane at room temperature. The ESA spectrum has been obtained from the transient spectrum of Figure 7 (see text for details) and is shifted by 28 330 cm^{-1}, the energy of the (0−0) $S_0 \rightarrow S_2$ transition.

TABLE 2: Band Centers (ν_0, × 10^3 cm^{-1}), Widths [Γ (fwhm), cm^{-1}], and Oscillator Strengths *f* of the Four Component Bands, A, B, C, and D, of the Observed Transient Spectrum $S_2 \rightarrow S_n$ Shown in Figure 7

	A	B	C	D
ν_0	17.7	19.1	23.1	25.2
Γ	1950	1220	3630	4540
f	1.8×10^{-3}	1×10^{-4}	7.4×10^{-4}	3.4×10^{-3}

Taking into account the origin of the $S_0 \rightarrow S_n$ absorption at 28 330 cm^{-1}, the ESA spectrum at 15 ps delay time may be compared in Figure 8 with the $S_0 \rightarrow S_n$ spectrum. Again, the 218 nm band has no $S_0 \rightarrow S_n$ counterpart. However, a transition of azulene, not obvious in absorption, has been observed at 217 nm (≈46 000 cm^{-1}) by MCD spectroscopy on its alkyl derivatives.[50] On the contrary, the second band around 190 nm closely matches the broad $S_0 \rightarrow S_n$ absorption centered at 190.5 nm (≈52 500 cm^{-1}).[51]

IV. Structure and Energetics of the S_0, S_1, and S_2 States

Ab initio calculations on azulene were performed with the GAMESS suite of programs[56,57] and using the 6-31G* basis set. The ground and lowest excited states (S_1 and S_2) were optimized at the MCSCF level, considering the complete active space (CAS) of 10 electrons distributed among the 10 lowest π molecular orbitals (hereafter designated CAS(10,10)). The total number of configurations amounts to 19 404. The stationary points determined by means of this procedure were classified as minimum or saddle points of the energy surface according to the number, 0 or 1, of imaginary frequencies found in the associated vibrational calculation. Vertical excitation energies, $\Delta E_{S_0 \rightarrow S_n}$, $\Delta E_{S_1 \rightarrow S_n}$, and $\Delta E_{S_2 \rightarrow S_n}$, and oscillator strengths *f* from the stationary points of the energy surfaces were then obtained. A perturbative correction, up to second order, was applied to the CAS energy of the ground and all excited states. This quantity takes into account the dynamical part of the electronic correlation and is calculated by means of the MCQDPT routine based on the quasi-degenerate perturbation theory (QDPT)[58−60]

TABLE 3: C−C Bondlengths (Å; Atom Numbering from Figure 1) at the Stationary Points of the Ground and of the Two Lowest Excited States of Azulene According to CAS(10,10)/6-31G* and DF/B3-LYP/6-31G* Calculations[a]

	S_0					S_1		S_2	
	C_{2v}	C_s	DF/B3-LYP	exp[b]		C_{2v}	C_s	C_{2v}	C_s
$r_{1,2}$	1.405	1.443	1.404	1.391	1.387	1.400	1.400	1.417	1.376
$r_{1,10}$	1.405	1.371	1.404		1.398	1.400	1.400	1.417	1.472
$r_{2,3}$	1.405	1.375	1.405	1.413	1.395	1.461	1.461	1.447	1.447
$r_{9,10}$	1.405	1.441	1.405		1.404	1.461	1.461	1.447	1.404
$r_{3,4}$	1.392	1.425	1.392	1.383	1.392	1.441	1.441	1.447	1.448
$r_{8,9}$	1.392	1.366	1.392		1.390	1.441	1.441	1.447	1.441
$r_{4,5}$	1.400	1.370	1.398	1.401	1.402	1.382	1.382	1.412	1.396
$r_{7,8}$	1.400	1.434	1.398		1.393	1.382	1.382	1.412	1.452
$r_{5,6}$	1.399	1.435	1.398	1.385	1.397	1.419	1.419	1.409	1.441
$r_{6,7}$	1.399	1.370	1.398		1.391	1.419	1.419	1.409	1.375
$r_{3,9}$	1.497	1.492	1.500	1.483	1.498	1.388	1.388	1.400	1.429

[a] All entries refer to CAS(10,10)/6-31G* calculations except when otherwise indicated. [b] From refs 70 and 71.

TABLE 4: Stationary Points of the Ground and of the Two Lowest Excited States of Azulene: E_{CAS}, Calculated Energy at the MCSCF/CAS(10,10)/6-31G* Level of Approximation; D_{QDPT}, Second-order Perturbative Correction to the CAS Energies; ΔE, Difference between Energies ($E_{CAS} + D_{QDPT}$) of Stationary Points; ΔE_{0-0}, Observed Energy Difference between the Ground and Excited State $v = 0$ Levels of C_{2v} Azulene; μ Equilibrium Dipole Moments of S_0, S_1, and S_2[a]

	CAS(10,10)				exp	
	E_{CAS}	μ	D_{QDPT}	ΔE	μ	ΔE_{0-0}
$S_0(C_{2v},1A_1)$[b]	−383.414961	0.704	−1.168169	0	0.79[c]	0
$S_0(C_s,1A')$	−383.415687	0.603	−1.162297	1.1		
$S_1(C_{2v},1B_2)$	−383.357298	−0.265	−1.162737	13.8	−0.42[d]	14.3[f]
$S_1(C_s,2A')$	−383.357298	−0.265	−1.162737	13.8		
$S_2(C_{2v},2A_1)$[e]	−383.263829	−0.446	−1.182198	30.1	−0.31[d]	28.8[g]
$S_2(C_s,3A')$	−383.269110	−0.296	−1.174901	30.5		

[a] All energy values are expressed in hartrees except ΔE and ΔE_{0-0} in 10^3 cm^{-1}. The dipole moments are expressed in debyes. [b] Saddle point with one b_2 imaginary frequency, 716i cm^{-1} at the CAS level of calculation. [c] From ref 72. [d] From ref 73. [e] Saddle point with one b_2 imaginary frequency, 3115i cm^{-1} at the CAS level of calculation. [f] From ref 74. [g] From ref 75.

and interfaced with the GAMESS program. Few other density functional (DF) calculations relative to S_0 were carried out with the Gaussian 98 program[61] using the B3-LYP exchange-correlation functional[62,63] and the 6-31G* basis set.

Our CASSCF(10,10)/6-31G* results on the ground and excited-state structures are reported in Tables 3 and 4. The ground state of azulene has been already studied by means of ab initio methods of varying accuracy in the past years in order to establish whether the bond-alternating or the bond-equalized structure, with C_s and C_{2v} symmetry, respectively, is at the energy minimum on the S_0 hypersurface.[21,64−69] In our case, the C_s equilibrium geometry is found to be more stable than C_{2v} by ≈160 cm^{-1}. The C_s stationary point is a minimum on the S_0 energy surface, being all associated vibrational frequencies real, and the C_{2v} structure a saddle point, having one b_2 imaginary frequency, 716i cm^{-1}. However, when the perturbative correction to the CAS energies is considered through the QDPT approach, the C_{2v} structure lowers at an energy below that of the C_s structure by ≈1140 cm^{-1}. In addition, the C_{2v} geometry is almost identical to that calculated by the DF approach (see Table 3) corresponding to a minimum on the S_0 energy surface (all of the vibrational frequencies are real). These are strong indications about C_{2v} symmetry of azulene in the ground state minimum. Only one equilibrium geometry is found for S_1: in fact, forcing the molecule to C_s symmetry, a structure is determined coincident within the computational accuracy with that optimized in C_{2v} symmetry. Finally, two critical points, one saddle (C_{2v}) and one minimum (C_s), have been determined for S_2, in close similarity with S_0. Also in this case, the QDPT treatment favors the C_{2v} structure over C_s by ≈400 cm^{-1} (see Table 4). Experimentally, no conclusive information on the molecular geometry comes from the X-ray diffraction data on the solid because of the disordered crystal arrangement.[70] On the contrary, the crystal structure of the azulene-*s*-trinitrobenzene complex has a small degree of disorder.[71] The geometry of azulene in the complex is substantially aromatic, i.e., with markedly reduced bond alternancy.[71] Table 3 shows that, while there is agreement between the C_{2v} and experimental[70,71] C−C bond lengths of S_0, a conspicuous discrepancy exists for the C_s values. In the S_1 state, the C_3−C_9 cross-link contracts strongly from 1.497 to 1.388 Å, whereas the adjacent C−C bonds lengthen, C_2−C_3 and C_9−C_{10} from 1.405 to 1.461 Å and C_3−C_4 and C_8−C_9 from 1.392 to 1.441 Å, as noted in previous calculations.[21,69] As for S_2, the C_{2v} structure has all C−C bonds of the ten-membered external ring elongated with respect to S_0 and the C_3−C_9 cross-link as short as 1.400 Å. The dipole moments of azulene in the S_0, S_1, and S_2 states depend on the molecular symmetry, as shown from Table 4 and compare satisfactorily with the experimental results.[72,73] Last, the QDPT-corrected energy values of the (0−0)S_0−S_1 and (0−0)S_0−S_2 transitions, relative to the C_{2v} structure of S_0, match closely the observed values.[74,75]

The nature of the two excited states, S_1 and S_2, deserves some other comments. The S_1 state is largely represented by singly excited configurations, and among these, the (HOMO;LUMO) has the largest weight (≈62%). As long as this single configuration is taken as representative of the S_1 state, the (HOMO;LUMO) $\pi\pi^*$ density is mostly centered between C atoms so that S_1 may be classified as a covalent state.[76] On the contrary, the contributions to S_2 from all singly excited configurations is smaller (≈50%) and more balanced, with preponderance of (HOMO;LUMO+1) and (HOMO-1;LUMO). It is still convenient, however, to classify the S_2 state as ionic because of these singly excited configurations, in close analogy with the nature of the second excited state of benzene.[76]

V. Discussion

All $\pi\pi^*$ excited states of C_{2v} azulene belong to A_1 or B_2 symmetry. Vertical excitation energies and oscillator strengths $S_0 \rightarrow S_n$ relative to the C_{2v} equilibrium geometry of S_0 have been calculated through the CAS(10,10)/6-31G* procedure and QDPT corrected. Data relative to those falling in the 16 000−44 000 cm^{-1} energy range, are compared with solution data in Table 5. When coupled with calculated oscillator strengths, they allow a straightforward assignment of the $S_0 \rightarrow S_n$ spectrum up to $S_8(3B_2)$, being the maximum deviation of calculated from experimental energies not larger than ≈1600 cm^{-1}.

Above 4 eV, there are states, weakly or not active in the $S_0 \rightarrow S_n$ spectrum, which may contribute to the ESA $S_1 \rightarrow S_n$ and $S_2 \rightarrow S_n$ spectra. We associate the $S_1 \rightarrow S_n$ spectrum to the equilibrium geometry of S_1. In fact, although the redistribution of the excess vibrational energy is far from complete within the short S_1 decay time, Franck-Condon factors from excited vibrational states will reasonably lead on the average to transient spectra similar to that originating from the equilibrium geometry of S_1. Therefore, vertical transitions $S_{1,eq}(1B_2) \rightarrow S_n$ have been calculated. Ab initio methods of comparable accuracy have been recently applied with good success to transient absorption in

TABLE 5: Calculated and Observed Vertical Excitation Energies ($\Delta E_{S_0 \rightarrow S_n}$, $\times 10^3$ cm^{-1}) and Oscillator Strengths, $f_{S_0 \rightarrow S_n}$, to the Lowest $\pi\pi^*$ States of Azulene[a]

	$\Delta E_{S_0 \rightarrow S_n}$		$f_{S_0 \rightarrow S_n}$	
	calc	exp	calc	exp
$S_1(1B_2)$	15.3	15.7	0.0025	0.009
$S_2(2A_1)$	29.5	29.2	0.0023	0.06[b]
$S_3(2B_2)$	32.2	33.7	0.016	≈0.03
$S_4(3A_1)$	38.4		0.11	
$S_5(4A_1)$	38.5	36.4	0.99	≈1.
$S_6(5A_1)$	38.7		0.075	
$S_7(6A_1)$	42.5		0.064	
$S_8(3B_2)$	42.7	42.1	0.10	0.4
$S_9(4B_2)$	43.5		4×10^{-5}	
$S_{10}(7A_1)$	44.1		0.547	
$S_{11}(5B_2)$	45.5		0.108	

[a] Calculated energies are relative to the S_0 C_{2v} equilibrium geometry, obtained through the MCSCF/CAS(10,10) procedure and QDPT corrected. Experimental oscillator strengths are from ref 48. [b] Two-thirds of this intensity are estimated to be borrowed through vibronic interactions, according to ref 48.

TABLE 6: Calculated and Observed Vertical Excitation Energies ($\Delta E_{S_1 \rightarrow S_n}$, $\times 10^3$ cm^{-1}) and Oscillator Strengths, $f_{S_1 \rightarrow S_n}$, to the Lowest $\pi\pi^*$ States of Azulene[a]

	$\Delta E_{S_1 \rightarrow S_n}$		$f_{S_1 \rightarrow S_n}$	
	calc	exp	calc	exp
$S_2(2A_1)$	16.2		0.0017	
$S_3(3A_1)$	20.3	22.3	0.037	1.5×10^{-4}[b]
$S_4(2B_2)$	21.3	18.9	1.5×10^{-5}	1×10^{-5}[c]
$S_5(4A_1)$	23.4		5.3×10^{-4}	
$S_6(5A_1)$	25.2	25.0	0.0035	1×10^{-4}[d]
$S_7(6A_1)$	27.9	26.5	0.007	2×10^{-4}[e]
$S_8(7A_1)$	29.5		2.5×10^{-4}	

[a] Calculated energies are relative to the S_1 equilibrium geometry, obtained through the MCSCF/CAS(10,10) procedure and QDPT corrected. [b] From Table 1, $f_B + f_C + f_D$. [c] From Table 1, f_A. [d] From Table 1, f_E. [e] From Table 1, f_F.

model systems.[36] In our case, there are three transitions with oscillator strengths much larger than all others up to ∼28 200 cm^{-1} above $S_{1,eq}$, namely, $S_{1,eq}(1B_2) \rightarrow S_3(3A_1)$, $S_{1,eq}(1B_2) \rightarrow S_6(5A_1)$, and $S_{1,eq}(1B_2) \rightarrow S_7(6A_1)$ (see Table 6). These states, i.e., $S_3(3A_1)$, $S_6(5A_1)$, and $S_7(6A_1)$, have been correlated with those responsible of the ground state absorption in Table 7 on the basis of their representation in terms of state eigenvectors. It may be seen from the same table that $S_3(3A_1)$, $S_6(5A_1)$, and $S_7(6A_1)$ (relative to the $S_{1,\,eq}$ geometry) correspond to $S_5(4A_1)$, $S_4(3A_1)$, and $S_7(6A_1)$ (relative to the S_0 geometry), respectively, being the components of each pair expressed by similar state eigenvectors. The $S_5(4A_1)$ state gives rise to the strongest band system of the $S_0 \rightarrow S_n$ spectrum of azulene. Our correlation indicates that this state is responsible of the 269 nm band in the spectrum of Figure 6, in agreement with the assignment of section III.A. On the contrary, evidence of other two states, not active in the $S_0 \rightarrow S_n$ absorption, comes only from the transient spectrum: the 26 500 cm^{-1} band is assigned to the $S_{1,eq}(1B_2) \rightarrow S_7(6A_1)$ transition, whereas the 25 000 cm^{-1} shoulder is assigned to the $S_{1,eq}(1B_2) \rightarrow S_6(5A_1)$ transition. The experimental/calculated energy difference is rather small for both transitions, <2000 cm^{-1}. These two bands, when shifted appropriately to take into account the origin of the $S_0 \rightarrow S_1$ absorption system, form the broad spectral feature around 244 nm in Figure 6. It is interesting to note that the $S_0 \rightarrow S_n$ MCD spectra of alkylazulenes show a second additional band with respect to those of azulene at ≈250 nm.[50] The latter, being in close agreement with the 250 nm shoulder of Figure 6, should thus be assigned as the $S_0 \rightarrow S_4(3A_1)$ transition.

TABLE 7: Excited States of Azulene: Coefficients of the Dominant Configurations (H = HOMO, L = LUMO, CAS(10,10)/MCSCF/6-31G* Results)[a]

@S_0		@$S_{1,eq}$		@$S_{2,eq}$		
$1B_2$	0.78	$1B_2$	0.79	$1B_2$	0.79	H;L
$2A_1$	0.44	$2A_1$	0.44	$2A_1$	0.42	H − 1;L
	0.5		0.42		0.46	H;L + 1
	0.25		0.28		0.25	$H^0;L^2$
$2B_2$	0.53	$2B_2$	0.49	$2B_2$	0.55	H − 1;L + 1
	0.45		0.44		0.41	H − 2;L
$3A_1$	0.35	$5A_1$	0.17	$4A_1$	0.26	H − 2;L + 1
	0.50		0.42		0.39	H − 1;L
	0.19		0.30		0.21	H − 4;L
	0.28		0.20		0.26	$H^0;(L+1)^2$
$4A_1$	0.64	$3A_1$	0.62	$5A_1$	0.64	H;L + 1
$5A_1$	0.43	$4A_1$	0.34	$3A_1$	0.36	H − 3;L
	0.31		0.51		0.40	$H^0;L^2$
	0.30		0.20		0.25	H − 1,H;L,L + 1
$6A_1$	0.44	$6A_1$	0.46	$7A_1$	0.47	$H^0;L^2$
	0.42		0.36		0.28	H − 1,H;L,L + 1
⋮	⋮	⋮	⋮	⋮	⋮	⋮
$5B_2$	0.31	$3B_2$	0.23	$5B_2$	0.15	H − 1;L + 1
	0.34		0.35		0.45	$H^0;L,L+1$
	0.46		0.35		0.50	$H-1,H;L^2$

[a] The excited states are defined at the equilibrium geometry of S_0, S_1 and S_2, i.e., @S_0, @$S_{1,eq}$, and @$S_{2,eq}$, respectively, and correlated on the basis of similar coefficients. The energy (eV) and the symmetry of the π and π^* molecular orbitals (6-31G* basis set) are as follows: −0.5249 (b_1;H − 4), −0.4464 (b_1;H − 3), −0.4013 (a_2;H − 2), −0.2929 (b_1;H − 1), −0.2532 (a_2;H), 0.058 (b_1;L), 0.0908 (a_2;L + 1), 0.2649 (b_1;L + 2), 0.3234 (b_1;L + 3), 0.3517 (a_2;L + 4).

TABLE 8: Calculated and Observed Vertical Excitation Energies ($\Delta E_{S_2 \rightarrow S_n}$, $\times 10^3$ cm^{-1}) and Oscillator Strengths, $f_{S_2 \rightarrow S_n}$, to the Lowest $\pi\pi^*$ States of Azulene[a]

	$\Delta E_{S_2 \rightarrow S_n}$		$f_{S_2 \rightarrow S_n}$	
	calc	exp	calc	exp
$S_3(2B_2)$	4.1		3×10^{-6}	
$S_4(3A_1)$	7.1		0.017	
$S_5(4A_1)$	11.5		3.2×10^{-4}	
$S_6(5A_1)$	12.0		2×10^{-5}	
$S_7(6A_1)$	12.1		3×10^{-5}	
$S_8(7A_1)$	12.2		1×10^{-5}	
$S_9(3B_2)$	13.9		6.5×10^{-4}	
$S_{10}(4B_2)$	14.6		2×10^{-5}	
$S_{11}(5B_2)$	15.2	17.7	0.033	1.9×10^{-3}[b]

[a] Calculated energies are relative to the S_2 C_{2v} equilibrium geometry, obtained through the MCSCF/CAS(10,10) procedure and QDPT corrected. [b] From Table 2, $f_A + f_B$.

The $S_2 \rightarrow S_n$ spectrum has been similarly calculated at the C_{2v} equilibrium geometry of S_2 (see Table 8). Only one transition, $S_{2,eq}(2A_1) \rightarrow S_{11}(5B_2)$, has a sufficiently large oscillator strength with respect to all others up to ≈24 200 cm^{-1}. Accordingly, the band observed 17 700 cm^{-1} and calculated 15 200 cm^{-1} above $S_{2,eq}$ is assigned to $S_{2,eq}(2A_1) \rightarrow S_{11}(5B_2)$. The $S_{11}(5B_2)$ state is correlated with the same state at the ground state geometry on the basis of Table 7. Following our considerations of Section III.B, the assignment is likely to hold also for the 217 nm MCD band of alkylazulenes.[50]

VI. Conclusions

In this paper, we have reported on the excited-state absorption of azulene in solution at room temperature using femtosecond pump−probe spectroscopy. The contributions to the transient spectrum from ground-state bleaching and stimulated emission have been evaluated and the resulting $S_1 \rightarrow S_n$ and $S_2 \rightarrow S_n$ ESA spectra have been discussed on the basis of ab initio CASSCF calculations and perturbative corrections to CAS energies.

As a major result of our study, transitions to higher lying $\pi\pi^*$ states have been observed which are in several cases not active in the ground-state absorption spectrum. Our calculations indicate that the states active in the $S_1 \rightarrow S_n$ spectrum are (i) one, $S_3(3A_1)$, responsible also of the strongest ground-state absorption and (ii) two close lying excited states, $S_7(6A_1)$ and $S_6(5A_1)$, which do not contribute significantly to the $S_0 \rightarrow S_n$ spectrum. As for the $S_2 \rightarrow S_n$ absorption, $S_{11}(5B_2)$, not seen in the $S_0 \rightarrow S_n$ spectrum but active in the MCD spectrum of the alkyl derivatives, is associated to the lowest ESA band.

This study, as well as a previous one,[30] emphasizes the fact that coupling of femtosecond transient absorption experiments with accurate ab initio calculations of excitation energies is a rewarding strategy to increase our understanding about excited-state energy surfaces.

Acknowledgment. This work was supported by the Italian Consiglio Nazionale delle Ricerche (CNR) and Ministero dell'Università e della Ricerca Scientifica e Tecnologica (MIUR) and by the European Community under the Contract HPRI-CT1999-00111. The authors thank CINECA (Bologna, Italy) for providing an allocation of computer time.

References and Notes

(1) Beer, M.; Longuet-Higgins, H. *J. Chem. Phys.* **1955**, *23*, 1390−1391.
(2) Sidman, J.; McClure, D. *J. Chem. Phys.* **1956**, *24*, 757−763.
(3) Huppert, D.; Jortner, J.; Rentzepis, P. M. *J. Chem. Phys.* **1972**, *56*, 4826−4833.
(4) Friedman, J. M.; Hochstrasser, R. M. *Chem. Phys.* **1974**, *6*, 145−154.
(5) Fujii, M.; Ebata, T.; Mikami, N.; Ito, M. *Chem. Phys.* **1983**, *77*, 191−200.
(6) Huppert, D.; Jortner, J.; Rentzepis, P. M. *Chem. Phys. Lett.* **1970**, *4*, 599−602.
(7) Rentzepis, P. *Chem. Phys. Lett.* **1969**, *3*, 717−720.
(8) Gillespie, G. D.; Lim, E. C. *J. Chem. Phys.* **1978**, *68*, 4578−4586.
(9) Berlman, I. *Handbook of Fluorescence Spectra of Aromatic Molecules*; Academic Press: New York, 1971.
(10) Wagner, B. D.; Tittelbach-Helmrich, D.; Steer, R. P. *J. Phys. Chem.* **1992**, *96*, 7904−7908.
(11) Gillespie, G. D.; Lim, E. C. *J. Chem. Phys.* **1976**, *65*, 4314−4316.
(12) Heritage, J. P.; Penzkofer, A. *Chem. Phys. Lett.* **1976**, *44*, 76−81.
(13) Ippen, F. P.; Shank, C. V.; Woerner, R. L. *Chem. Phys. Lett.* **1977**, *46*, 20−23.
(14) Shank, C. V.; Ippen, F. P.; Teschke, O.; Fork, R. D. *Chem. Phys. Lett.* **1978**, *57*, 433−434.
(15) Schwarzer, D.; Troe, J.; Schroeder, J. *Ber. Bunsen-Ges. Phys. Chem.* **1991**, *95*, 932−934.
(16) Matsumoto, T.; Ueda, K.; Tomita, M. *Chem. Phys. Lett.* **1992**, *191*, 627−632.
(17) Tittelbach-Helmrich, D.; Wagner, B. D.; Steer, R. P. *Chem. Phys. Lett.* **1993**, *209*, 464−468.
(18) Wagner, B. D.; Szymanski, M.; Steer, R. P. *J. Chem. Phys.* **1993**, *98*, 301−307.
(19) Tittelbach-Helmrich, D.; Wagner, B. D.; Steer, R. P. *Can. J. Chem.* **1995**, *73*, 303−306.
(20) Wurzer, A. J.; Wilhelm, T.; Piel, J.; Riedle, E. *Chem. Phys. Lett.* **1999**, *299*, 296−302.
(21) Bearpark, M. J.; Bernardi, F.; Clifford, S.; Olivucci, M.; Robb, M. A.; Smith, B. R.; Vreven, T. *J. Am. Chem. Soc.* **1996**, *118*, 169−175.
(22) Ruth, A. A.; Kim, E.-K.; Hese, A. *Phys. Chem. Chem. Phys.* **1999**, *1*, 5121−5128.
(23) Fleming, G. *Chemical Applications of Ultrafast Spectroscopy*; Oxford University Press: New York, 1986.
(24) Brückner, V.; Feller, K.-H.; Grummt, U.-W. *Applications of time-resolved optical spectroscopy*; Elsevier: Amsterdam, 1990.
(25) Manz, J.; Wöste, L. *Femtosecond Chemistry*; VCH: Weinheim, 1995.
(26) Neuwhal, F. V. R.; Bussotti, L.; Foggi, P. In *Res. Adv. Photochem. Photobiol., vol. 1*; Global Research Network: Trivandrum, India, 2000; pp 77−94.
(27) Elsaesser, T.; Kaiser, W. *Annu. Rev. Phys. Chem.* **1991**, *42*, 83−107.
(28) Pollard, W. T.; Mathies, R. A. *Annu. Rev. Phys. Chem.* **1992**, *43*, 497−523.
(29) Foggi, P.; Pettini, L.; Santa, I.; Righini, R.; Califano, S. *J. Phys. Chem.* **1995**, *99*, 7439−7445.
(30) Bussotti, L.; Foggi, P.; Gellini, C.; Moroni, L.; Salvi, P. R. *Phys. Chem. Chem. Phys.* **2001**, *3*, 3027−3033.
(31) Buntinx, G.; Naskrecki, R.; Poizat, O. *J. Phys. Chem.* **1996**, *100*, 19380−19388.
(32) Lednev, I. K.; Ye, T.-Q.; Hester, R. E.; Moore, J. H. *J. Phys. Chem.* **1996**, *100*, 13338−13341.
(33) Neuwhal, F. V. R.; Foggi, P.; Brown, R. *Chem. Phys. Lett.* **2000**, *319*, 157−163.
(34) Kovalenko, S. A.; Eilers-Konig, N.; Senyushkina, T. A.; Ernsting, N. P. *J. Phys. Chem. A* **2001**, *105*, 4834−4843.
(35) Neuwhal, F. V. R.; Righini, R.; Dei, A. *Chem. Phys. Lett.* **2002**, *352*, 408−414.
(36) Cronstrand, P.; Christiansen, O.; Norman, P.; Agren, H. *Phys. Chem. Chem. Phys.* **2000**, *2*, 5357−5363.
(37) Perkampus, H.-H. *UV−Vis Atlas of Organic Compunds*; VCH: Weinheim, Germany, 1992.
(38) Danielius, R.; Piskarkas, A.; Trapani, P. D.; Andreoni, A.; Solcia, L.; Foggi, P. *Appl. Opt.* **1996**, *35*, 5336−5339.
(39) Ciano, L.; Foggi, P.; Salvi, P. R. *J. Photochem. Photobiol. A* **1997**, *105*, 129−134.
(40) Heilbronner, E. In *Non-Benzenoid Aromatic Compounds*; Interscience Publishers: New York, 1959; pp 171−276.
(41) Mann, D. E.; Platt, J. R.; Klevens, H. E. *J. Chem. Phys.* **1949**, *17*, 481−484.
(42) Sidman, J. W.; McClure, D. S. *J. Chem. Phys.* **1956**, *24*, 757−763.
(43) Hunt, G. R.; Ross, I. G. *J. Mol. Spectrosc.* **1962**, *9*, 50−78.
(44) Lacey, A. R.; McCoy, E. F.; Ross, I. G. *Chem. Phys. Lett.* **1973**, *21*, 233−241.
(45) Small, G. J.; Kusserow, S. *J. Chem. Phys.* **1974**, *60*, 1558−1563.
(46) Dekkers, H. P. J. M.; Westra, S. W. T. *Mol. Phys.* **1975**, *30*, 1795−1811.
(47) Zimmermann, H.; Joop, N. *Z. Elektrochem., Ber. Bunsen-Ges. Phys. Chem.* **1960**, *64*, 1219−1221.
(48) Thulstrup, E. W.; Case, P. L.; Michl, J. *Chem. Phys.* **1974**, *6*, 410−418.
(49) Tajiri, A.; Hatano, M. *Chem. Phys. Lett.* **1975**, *34*, 29−33.
(50) Gerhartz, W.; Michl, J. *J. Am. Chem. Soc.* **1978**, *100*, 6877−6881.
(51) Kourouklis, G. A.; Siomos, K.; Christophorou, L. G. *J. Mol. Spectrosc.* **1982**, *92*, 127−140.
(52) Lewis, J. W.; Nauman, R. V.; D. B. Bouler, J.; McGlynn, S. P. *J. Phys. Chem.* **1983**, *87*, 3611−3615.
(53) Chao, R. S.; Khanna, R. K. *Spectrochim. Acta* **1977**, *33A*, 53−62.
(54) Wild, W.; Seilmeier, A.; Gottfried, N. H.; Kaiser, W. *Chem. Phys. Lett.* **1985**, *119*, 259−263.
(55) Schwarzer, D.; Troe, J.; Votsmeier, M.; Zerezke, M. *J. Chem. Phys.* **1996**, *105*, 3121−3131.
(56) Dupuis, M.; Spangler, D.; Wendoloski, J. J. *NRCC Software Catalog, vol.1, program n. QG01, GAMESS.*; 1980.
(57) Schmidt, M. W.; Baldridge, K. K.; Boatz, J. A.; Elbert, S. T.; Gordon, M. S.; Jensen, J. H.; Koseki, S.; Matsunaga, N.; Nguyen, K. A.; Su, S. J.; Windus, T. L.; Dupuis, M.; Montgomery, J. A. *J. Comput. Chem.* **1993**, *14*, 1347−1363.
(58) Nakano, H. *J. Chem. Phys.* **1993**, *99*, 7983−7992.
(59) Nakano, H. *Chem. Phys. Lett.* **1993**, *207*, 372−378.
(60) Nakano, H.; Yamanishi, M.; Hirao, K. *Trends Chem. Phys.* **1997**, *6*, 167−214.
(61) Frisch, M. J.; Trucks, G. W.; Schlegel, H. B.; Scuseria, G. E.; Robb, M. A.; Cheeseman, J. R.; Zakrzewski, V. G.; Montgomery, J. A., Jr.; Stratmann, R. E.; Burant, J. C.; Dapprich, S.; Millam, J. M.; Daniels, A. D.; Kudin, K. N.; Strain, M. C.; Farkas, O.; Tomasi, J.; Barone, V.; Cossi, M.; Cammi, R.; Mennucci, B.; Pomelli, C.; Adamo, C.; Clifford, S.; Ochterski, J.; Petersson, G. A.; Ayala, P. Y.; Cui, Q.; Morokuma, K.; Malick, D. K.; Rabuck, A. D.; Raghavachari, K.; Foresman, J. B.; Cioslowski, J.; Ortiz, J. V.; Stefanov, B. B.; Liu, G.; Liashenko, A.; Piskorz, P.; Komaromi, I.; Gomperts, R.; Martin, R. L.; Fox, D. J.; Keith, T.; Al-Laham, M. A.; Peng, C. Y.; Nanayakkara, A.; Gonzalez, C.; Challacombe, M.; Gill, P. M. W.; Johnson, B. G.; Chen, W.; Wong, M. W.; Andres, J. L.; Head-Gordon, M.; Replogle, E. S.; Pople, J. A. *Gaussian 98*, revision A.9; Gaussian, Inc.: Pittsburgh, PA, 1998.
(62) Becke, A. D. *J. Chem. Phys.* **1993**, *98*, 5648−5652.
(63) Lee, C.; Yang, W.; Parr, R. G. *Phys. Rev. B* **1988**, *37*, 785−789.
(64) Kollmar, H. *J. Am. Chem. Soc.* **1979**, *101*, 4832−4840.
(65) Haddon, R. C.; Raghavachari, K. *J. Am. Chem. Soc.* **1982**, *104*, 3516−3518.
(66) Glidewell, C.; Lloyd, D. *Tetrahedron* **1984**, *40*, 4455−4472.
(67) Schulman, J. M.; Peck, R. C.; Disch, R. L. *J. Am. Chem. Soc.* **1989**, *111*, 5675−5680.
(68) Grimme, S. *Chem. Phys. Lett.* **1993**, *201*, 67−74.

(69) Negri, F.; Zgierski, M. Z. *J. Chem. Phys.* **1993**, *99*, 4318−4326.
(70) Robertson, J. M.; Shearer, H. M. M.; Sim, G. A.; Watson, D. G. *Acta Crystallogr.* **1962**, *15*, 1−8.
(71) Hanson, A. W. *Acta Crystallogr.* **1965**, *19*, 19−26.
(72) Tobler, H. J.; Bauder, A.; Gunthard, H. H. *J. Mol. Spectrosc.* **1965**, *18*, 239−246.
(73) Hochstrasser, R. M.; Noe, L. J. *J. Chem. Phys.* **1969**, *50*, 1684−1688.
(74) Amirav, A.; Jortner, J. *J. Chem. Phys.* **1984**, *81*, 4200−4205.
(75) Fujii, M.; Ebata, T.; Mikami, N.; Ito, M. *Chem. Phys.* **1983**, *77*, 191−200.
(76) Craig, M.; Berry, R. S. *J. Am. Chem. Soc.* **1967**, *89*, 2801−2805.